Robotica (2004) volume 22, pp. 163–171. © 2004 Cambridge University Press
DOI: 10.1017/S0263574703005423 Printed in the United Kingdom

Combined force and visual control of an industrial robot

Ricardo Carelli, Eduardo Oliva, Carlos Soria and Oscar Nasisi

Instituto de Auntomática (INAUT), Facultad de Ingeniería, Universidad Nacional de San Juan, Av. San Martin Oeste 1109, San Juan (5400) (Argentina).
E-mail: rcarelli@inaut.unsj.edu.ar

(Received in Final Form: June 11, 2003)

SUMMARY
This work proposes control structures that efficiently combine force control with vision servo control of robot manipulators. Impedance controllers are considered which are based both on visual servoing and on physical or fictitious force feedback, the force and visual information being combined in the image space. Force and visual servo controllers included in extended hybrid control structures are also considered. The combination of both force and vision based control allows the tasks range of the robot to be extended to partially structured environments. The proposed controllers, implemented on an industrial SCARA-type robot, are tested in tasks involving physical and virtual contact with the environment.

KEYWORDS: Robot manipulators; Visual servoing; Impedance control; Force control; Hybrid control.

1. INTRODUCTION

A fundamental requirement for the success of any robotic task is the capability of the robot manipulator to interact with the work environment, which calls for its precise modelling. However, it is not always possible or convenient to consider a structured environment. If so, it is necessary to obtain exteroceptive sensorial information that may satisfy a precise interaction of the robot with its environment. Mechanical interaction tasks can be achieved by measuring the contact forces of the end-effector. Various force control schemes have been proposed including pure-force control, impedance control, hybrid control and parallel control.[1–3] A review of force control in robotics is presented in De Schutter et al.,[4] Chiaverini and Siciliano[5] and Yoshikawa.[6] Information supplied by vision cameras, either fixed or mounted on the manipulator, is important for tasks that require to approximate or to position the robot with respect to the environment. Visual servoing has been proposed for robot guidance based on visual information.[7–9] Castaño and Hutchinson[10] propose a combination of visual feedback control and control with internal position sensors conforming a structure of hybrid control, which uses a fixed camera. In Tsuji et al.,[11] a non-contact impedance control for a redundant robot is proposed, which uses the visual information provided by a fixed camera to generate a virtual force between each robot joint and an object in the environment. In Nakabo and Ishikawa,[12] a concept of visual contact using a fixed camera is introduced, which defines a virtual contact with a virtual surface on the image. The system is dynamically implemented with a *1 ms* sampling period. In Mut et al.[13] a visual impedance controller for hand-mounted camera is presented, based on fictitious interaction forces generated from the image and capable of adapting to dynamic uncertainties of the robot.

Recently proposed schemes combine both visual and physical force information into hybrid or impedance control structures that aim at increasing the performance capability of a robot in partially structured environments. Morel et al.[14] have proposed a control structure in which, by means of a camera mounted on the robot's end-effector, the visual controller may generate references for a conventional impedance control with physical force feedback. The system is tested in an insertion task where the visual control contributes to robot approximation and the impedance control accommodates the robot during the insertion itself. In Nelson et al.,[15] a hybrid force and visual controller is proposed. Hosoda et al.,[16], considers an adaptive force and vision based hybrid controller capable of estimating the parameters both of the camera and of the contact surface.

This paper proposes two impedance control structures based on visual servo control and on feedback either from the measured physical force or from a fictitious force obtained through the visual information. These structures are designed for a camera-in-hand robot, and have the characteristic of performing the control directly on the image plane. That is, the force – either physical or fictitious – generates a correction signal on the vision references. These schemes allow for the robot interaction control either with or without contact within partially structured environments. Moreover, the work proposes to combine these controllers with both pure-force control and motion control into a hybrid control scheme, based on a set of controllers that are adequately selected depending on the task to perform. This allows for a greater versatility and, therefore, a possibility to carry out a wide range of tasks with a high autonomy level. The proposed control systems have been implemented on a SCARA industrial robot, and experiments have been carried out both with insertion and with motion that avoids visually detected objects. The objective of developing controllers that are applicable to available industrial robots aims at facilitating their use in industrial applications.

The paper is organized as follows. Section 2 describes the proposed visual servo controller. In Section 3, the vision based impedance control strategy is presented, and in

https://doi.org/10.1017/S0263574703005423 Published online by Cambridge University Press

Section 4 the hybrid control structure is described. Section 5 presents the industrial robot model considered in the experiments. Section 6 is devoted to the experimental results and finally, Section 7 offers some concluding remarks.

2. VISUAL SERVO CONTROL

2.1 Control Law

The visual servo controller considered here for an industrial robot is based on the position visual controller proposed by the authors in Kelly et al.[9] for a camera-in-hand robot manipulator. This controller has been experimented on a direct-drive actuated manipulator, generating the torque references for each joint. The control law is structured as a transposed Jacobian controller.[17] Its simple structure is based on the direct feedback of image features errors and of the joint positions and speeds. In particular, image features are defined as p points of interest, identified on the image plane and associated to the vector $\boldsymbol{\xi} \in \Re^{2p}$ of the corresponding coordinates in the reference system of the image. That is, each point of interest in the workspace, or feature point ${}^C\mathbf{p}_o$ with coordinates $[{}^Cp_{xo}\ {}^Cp_{yo}\ {}^Cp_{zo}]^T$ in a reference system associated to the camera, is projected on the image plane with coordinates $[u\ v]^T$ (Figure 1). These coordinates for all of the p feature points defined on the object of interest and projected on the image plane, constitute the vector of image features $\boldsymbol{\xi} \in \Re^{2p}$.

In this way, the robot task is specified on the image plane in terms of the image features. The control problem is now reduced to designing a controller that calculates the voltage levels to be applied to the motors, so that the motion of the robot end-effector will allow the desired feature vector $\boldsymbol{\xi}_d$ to be reached on the image plane of the camera mounted on the manipulator's hand, which corresponds to a desired relative position between the robot and the object of interest. That is,

$$\lim_{t\to\infty} \xi(t) = \xi_d \tag{1}$$

In the present work, the controller is defined as,

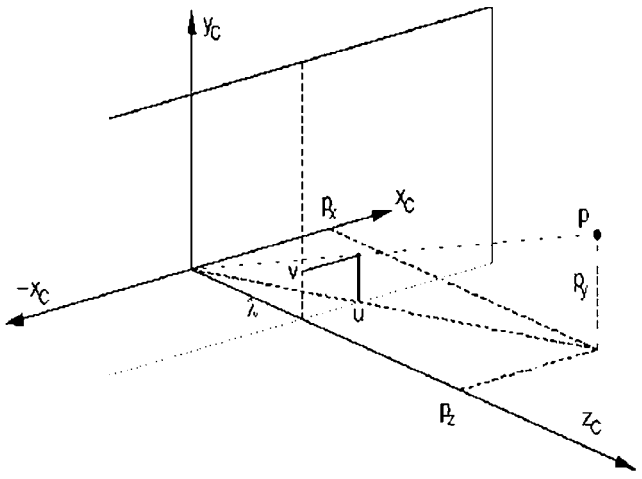


Fig. 1. Projection of an object point on the image plane.

$$\mathbf{v} = \mathbf{J}(\mathbf{q}, \boldsymbol{\xi}, {}^C\mathbf{p}_z)^T\ \mathbf{K}_p\tilde{\boldsymbol{\xi}} - \mathbf{K}_v\dot{\mathbf{q}} \tag{2}$$

where $\mathbf{q}, \dot{\mathbf{q}} \in \Re^n$ are the robot joint position and velocity vectors; $\boldsymbol{\xi} \in \Re^{2p}$ the image features vector, assuming there are p points of interest; $\tilde{\boldsymbol{\xi}} = \boldsymbol{\xi}_d - \boldsymbol{\xi}$ the features error vector on the image plane; ${}^C\mathbf{p}_z$ the visual depth between the camera and object – assumed to be known; $\mathbf{v} \in \Re^n$ is the control signal represented by the voltage supplied onto the robot's dc actuators. Besides, $\mathbf{K}_p \in \Re^{2p\times 2p}$, $\mathbf{K}_v \in \Re^{n\times n}$ are positive definite and symmetric gain matrices to be chosen by the designer. Finally, $\mathbf{J}$ is the Jacobian matrix defined as the product between the image Jacobian matrix[1] $\mathbf{J}_I$ and the analytical Jacobian matrix[9] of the manipulator $\mathbf{J}_R$,

$$\mathbf{J}(\mathbf{q}, \boldsymbol{\xi}, {}^Cp_z) = \mathbf{J}_I(\boldsymbol{\xi}, {}^C\mathbf{p}_z)\mathbf{J}_R(\mathbf{q}) \tag{3}$$

The Jacobian relates time derivatives $\dot{\mathbf{q}}$, $\dot{\boldsymbol{\xi}}$ as

$$\dot{\boldsymbol{\xi}} = \mathbf{J}(\mathbf{q}, \boldsymbol{\xi}, {}^C\mathbf{p}_z)\dot{\mathbf{q}}. \tag{4}$$

A detailed description of the image Jacobian is given in Kelly et al.[9] The controller represented by (2) requires that both the joint position and joint velocity vectors be measured as well as the error in the image plane, and that the Jacobian matrix be known. Figure 2 shows the structure of the visual servo controller.

2.2 Stability Analysis

In Kelly et al.[9] the authors have presented a visual servo controller with stability proof that considers the non-linear and coupled dynamics of a rigid robot manipulator. The present paper is mainly oriented to the control of a rigid n-link industrial robot. It is assumed that the industrial robot's transmission reduction ratios are high and, hence, the linear motor dynamics dominate over the arm's non-linear dynamics. Moreover, the electrical dynamics of the servomotors are sufficiently fast as to be ignored. For such assumptions on the industrial robot, and considering that the voltages applied to the dc drives are the input variables, the typically dominant dynamics can be represented by the following linear equation,

$$\mathbf{M}\ddot{\mathbf{q}} + \mathbf{F}\dot{\mathbf{q}} + \mathbf{D}\boldsymbol{\tau} = \mathbf{G}\mathbf{v} \tag{5}$$

where $\mathbf{M} \in \Re^{n\times n}$ represents the diagonal matrix of dominant motor inertias, $\mathbf{F} \in \Re^{n\times n}$ represents the linear friction coefficients; $\mathbf{D} \in \Re^{n\times n}$ is the diagonal gain matrix relating disturbance torques on the links to those on the motor side, and $\mathbf{G} \in \Re^{n\times n}$ is a gain diagonal matrix relating input voltages $\boldsymbol{v}$ to torques on the motors. Finally, $\mathbf{q}$, $\dot{\mathbf{q}}$ and $\ddot{\mathbf{q}}$ are $\Re^n$ vectors of joint position, velocity and acceleration, respectively. The dynamical model of (5) is explained in detail for a SCARA robot in Section 5.

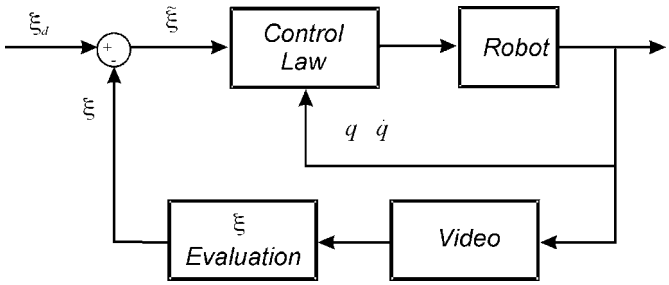


Fig. 2. Visual servo control diagram.

https://doi.org/10.1017/S0263574703005423 Published online by Cambridge University Press

By equating (2) and (5) and disregarding the disturbance term in (5), the following closed-loop non-linear equation is obtained,

$$\mathbf{M}\ddot{\mathbf{q}}+\mathbf{F}\dot{\mathbf{q}}=\mathbf{G}[\mathbf{J}(\mathbf{q},\,\boldsymbol{\xi},\,{}^{C}\mathbf{p}_z)^T\mathbf{K}_p\boldsymbol{\xi}-\mathbf{K}_v\dot{\mathbf{q}}\} \tag{6}$$

The state vector $[\mathbf{q}^T\ \dot{\mathbf{q}}^T]^T$ is considered in this equation. Now, as in the previous paper,[9] we make the following assumptions.

Assumptions:

A1. The object in the workspace is static.

A2. There exists a robot joint configuration $\boldsymbol{q}_d$ for which the feature error vanishes, $\boldsymbol{\xi}_d=\boldsymbol{\xi}(\mathbf{q}_d)$.

A3. The unknown desired joint position $\boldsymbol{q}_d$ is an isolated solution of $\boldsymbol{\xi}(\mathbf{q})=\boldsymbol{\xi}_d$.

A4. The Jacobian (3), $\mathbf{J}(\mathbf{q},\ \boldsymbol{\xi}(\mathbf{q}),\ {}^{C}p_z(\mathbf{q}))$, is continuously differentiable with respect to each entry $\boldsymbol{q}$ and,

$$rank\{\mathbf{J}(\mathbf{q}^d,\ \boldsymbol{\xi}(\mathbf{q}_d),\ {}^{C}\mathbf{p}_z(\mathbf{q}_d))\}=n.$$

A5. The distance ${}^{C}\mathbf{p}_z$ from camera to object (depth) is known.

Assumption A1 sets a positioning servo control problem. A2 assures that the control problem is solvable. A3 is a necessary condition to set up stability in an asymptotic sense. This is equivalent to assuming that the robot does not have any kinematic redundancy with respect to the visual task. Assumption A4 is required for the stability analysis. A necessary condition to meet A4 is to select the number of object points p such that $2p\geq n$ and, hereafter, this is supposed to be the case. Concerning A5, the knowledge of the distance between the camera and the object in the workspace is reduced, in the applications performed in this paper with a SCARA robot, to that of the constant distance between the camera and the work plane.

The following lemma, necessary for the stability analysis, is considered.

Lemma 1: Considering assumptions A1–A4, the equation

$$\mathbf{J}(\mathbf{q},\ \boldsymbol{\xi}(\mathbf{q}),\ {}^{C}\mathbf{p}_z(\mathbf{q}))^T\mathbf{K}_p[\boldsymbol{\xi}_d-\boldsymbol{\xi}(\mathbf{q})=0$$

has an isolated solution at $\mathbf{p}=\mathbf{q}_d$.

Proof: From the assumptions A2–A4, $rank\{\mathbf{J}(\mathbf{q},\boldsymbol{\xi}(\mathbf{q}),\ {}^{C}\mathbf{p}_z(\mathbf{q}))\}=n$ for all $\mathbf{q}$ in a neighbourhood of $\mathbf{q}_d$. Taking this into account, along with the fact that $\mathbf{K}_p$ is a square non-singular matrix ($rank\{\mathbf{K}_p\}=2p$), $rank\{\mathbf{J}(\mathbf{q},\boldsymbol{\xi}(\mathbf{q}),\ {}^{C}\mathbf{p}_z(\mathbf{q}))\mathbf{K}_p\}=n$ in a neighbourhood of $\mathbf{q}_d$. Now, considering assumptions A3 and A4, by recalling the mean-value theorem applied to (4), $\boldsymbol{\xi}_d-\boldsymbol{\xi}(\mathbf{q})=\mathbf{J}(\bar{\mathbf{q}},\boldsymbol{\xi}(\bar{\mathbf{q}}),\ {}^{C}\mathbf{p}_z(\bar{\mathbf{q}}))[\mathbf{q}_d-\mathbf{q}]$, with some $\bar{\mathbf{q}}$ in the neighbourhood of $\mathbf{q}_d$. Therefore, $\mathbf{J}(\mathbf{q},\ \boldsymbol{\xi},\ {}^{C}\mathbf{p}_z)^T\mathbf{K}_p[\boldsymbol{\xi}_d-\boldsymbol{\xi}]=0$ can be rewritten as

$$\mathbf{J}(\bar{\mathbf{q}},\ \boldsymbol{\xi}(q),\ {}^{C}\mathbf{p}_z(q))^T\mathbf{K}_p\mathbf{J}(\bar{\mathbf{q}},\ \boldsymbol{\xi}(\bar{\mathbf{q}}),\ {}^{C}\mathbf{p}_z(\bar{\mathbf{q}}))[\mathbf{q}_d-\mathbf{q}]=0. \tag{7}$$

On the other hand, it should be noted that, for all $\bar{\mathbf{q}}$ in the neighbourhood of $\mathbf{q}_d$,

$$\mathbf{J}(\bar{\mathbf{q}},\ \boldsymbol{\xi}(\bar{\mathbf{q}}),\ {}^{C}\mathbf{p}_z(\bar{\mathbf{q}}))^T\mathbf{K}_p\mathbf{J}(\bar{\mathbf{q}},\ \boldsymbol{\xi}(\bar{\mathbf{q}}),\ {}^{C}\mathbf{p}_z(\bar{\mathbf{q}})) \tag{8}$$

is a symmetric positive definite matrix because $rank\{\mathbf{J}(\bar{\mathbf{q}},\ \boldsymbol{\xi}(\bar{\mathbf{q}}),\ {}^{C}\mathbf{p}_z(\bar{\mathbf{q}})]=n$, $\mathbf{K}_p$ is a symmetric non-singular matrix, and $2p\geq n$. Since (7) is a positive-definite matrix and, hence, also non-singular, then by the continuity established in assumption A4, it can be stated that

$$\mathbf{J}(\mathbf{q},\ \boldsymbol{\xi}(\mathbf{q}),\ {}^{C}\mathbf{p}_z(\mathbf{q}))^T\mathbf{K}_p\mathbf{J}(\bar{\mathbf{q}},\ \boldsymbol{\xi}(\bar{\mathbf{q}}),\ {}^{C}\mathbf{p}_z(\bar{\mathbf{q}}))$$

is also a square non-singular matrix for all $\mathbf{q}$ and $\bar{\mathbf{q}}$ in a neighbourhood of $\mathbf{q}_d$. This allows to conclude that $\mathbf{q}=\mathbf{q}_d$ is a unique solution for (7) in a sufficiently small neighbourhood of $\mathbf{q}_d$.

For the stability analysis, the Lyapunov's direct method[19] is used; thus the following Lyapunov candidate function is proposed,

$$\begin{aligned}V&=\tfrac{1}{2}\dot{\mathbf{q}}^T(\mathbf{G}^{-1}\mathbf{M})\dot{\mathbf{q}}+\tfrac{1}{2}[\boldsymbol{\xi}(\mathbf{q}_d)-\boldsymbol{\xi}(\mathbf{q})]^T\ \mathbf{K}_p[\boldsymbol{\xi}(\vartheta_d)-\boldsymbol{\xi}(\mathbf{q})]\\&=\tfrac{1}{2}\dot{\mathbf{q}}^T(\mathbf{G}^{-1}\mathbf{M})\dot{\mathbf{q}}+\tfrac{1}{2}\tilde{\boldsymbol{\xi}}^T\mathbf{K}_p\tilde{\boldsymbol{\xi}}\end{aligned} \tag{9}$$

which, according to assumption A3, is a locally positive-definite function. The time derivative of (9) is,

$$\dot{V}=\dot{\mathbf{q}}^T(\mathbf{G}^{-1}\mathbf{M})\ddot{\mathbf{q}}-\tilde{\boldsymbol{\xi}}^T\mathbf{K}_p\boldsymbol{\xi}$$

By substituting $\mathbf{G}^{-1}\mathbf{M}\ddot{\mathbf{q}}$ from equation (6) and taking into account (4),

$$\dot{V}=-\dot{\mathbf{q}}^T(\mathbf{K}_v+\mathbf{G}^{-1}\mathbf{F})\dot{\mathbf{q}}\leq 0 \tag{10}$$

is obtained, which is a semi-definite negative function, thus implying stability of the equilibrium $[\mathbf{q}_d^T\ \mathbf{0}^T]^T$. Since the system in (6) is autonomous, it is possible to apply the LaSalle theorem[19] to analyse the local asymptotic stability. In order to do this, the region

$$\Omega=\left\{\begin{bmatrix}\mathbf{q}\\ \dot{\mathbf{q}}\end{bmatrix}:\dot{V}(\mathbf{q},\ \dot{\mathbf{q}})=0\right\}$$

is defined. The major invariant set in Ω is given by $\dot{\mathbf{q}}=\mathbf{0}$, $\mathbf{q}\in\Re^n$: $\mathbf{J}^T\mathbf{K}_p\tilde{\boldsymbol{\xi}}=\mathbf{0}$. Furthermore, according to *Lemma 1*, the latter equation is satisfied for $\mathbf{q}=\mathbf{q}_d$. Therefore, by invoking the LaSalleś theorem, it can be assure that the equilibrium $[\mathbf{q}^T\dot{\mathbf{q}}^T]^T=[\mathbf{q}_d^T\mathbf{0}^T]^T$ is locally asymptotically stable. This means that the control objective is reached, $\lim^{t\rightarrow\infty}\ \boldsymbol{\xi}(t)=\mathbf{0}$ for a sufficiently small initial feature error $\tilde{\boldsymbol{\xi}}(0)$ and joint velocity $\dot{\mathbf{q}}(0)$.

3. VISION BASED IMPEDANCE CONTROL

In robotics, the concept of impedance control[18] is aimed at the dynamic regulation between the motion and the interacting force of the robot with the environment. Linear impedance can be expressed through Laplace transform as,

$$\mathbf{Z}(s)\tilde{\mathbf{x}}(s)=\mathbf{f}(s) \tag{11}$$

where $\mathbf{f}$ is the interacting force of the robot with the environment, $\tilde{\mathbf{x}}=\mathbf{x}_d-\mathbf{x}$ represents the robot's motion error in relation to the specified trajectory $\mathbf{x}_d(t)$ in the workspace, and $\mathbf{Z}(s)$ is the impedance function.

A way to implement the impedance controller[1] is through the scheme called internal motion loop impedance control (Figure 3). As shown in the figure, the impedance external loop generates deviations to the motion reference of the internal loop. The deviation vector $\mathbf{x}_a$ is obtained by filtering the interaction forces according to,

$$\mathbf{x}_a(t)=[\mathbf{I}p^2+\mathbf{B}p+\mathbf{K}]^{-1}\mathbf{f}(t) \tag{12}$$

where $\mathbf{I}\in\Re^{n\times n}$ is called the inertia matrix, $\mathbf{B}\in\Re^{n\times n}$ the damping matrix, $\mathbf{K}\in\Re^{n-n}$ the elasticity matrix, and p is the

https://doi.org/10.1017/S0263574703005423 Published online by Cambridge University Press

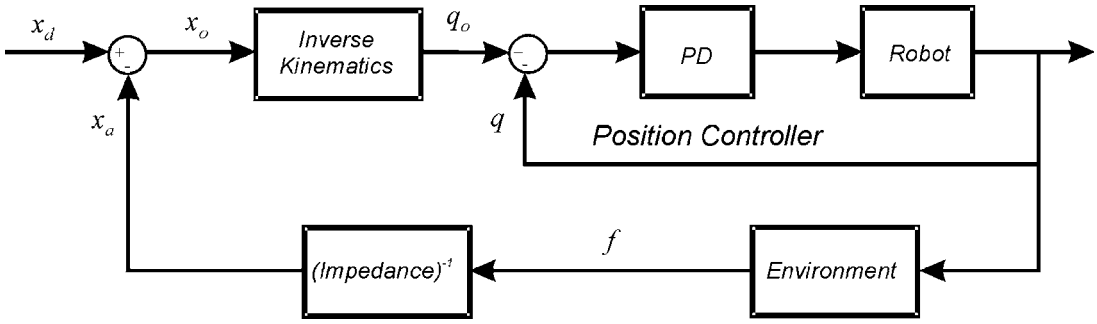


Fig. 3. Impedance control scheme.

time derivative operator. **I**, **B**, **K** are real, positive-definite diagonal matrices that characterize the desired impedance function and they are specified according to the desired dynamic interaction behaviour of the robot.

Some authors have extended this scheme to the vision servo control. In Morel,[14] the structure of Figure 3 is added an external vision based control loop that generates the references for the impedance controller with feedback of physical forces. Nakabo and Ishikawa[12] proposes to use fictitious forces that act by modifying the control signals generated by a conventional motion controller, from the images captured by a fixed camera external to the robot for non-contact approximation tasks. Besides, Tsuji et al.[11] proposes a non-contact impedance control for a redundant robot using the visual information from a fixed camera to generate the virtual force between each robot joint and an object in the environment.

The present work considers an impedance control structure where the fusion of information from forces – either physical or virtual – with the visual servo control is performed directly on the image plane of a camera mounted on the robot hand. Physical forces are considered when trying to regulate the mechanical interaction by using information from vision and force sensors. Fictitious forces are used when a non-contact regulation is preferred, that is, a virtual interaction captured by the image. The control objective is then defined as the regulation of the dynamic relationship between the physical or fictitious forces and the image features error on the image plane,

$$\mathbf{Z}(s)\boldsymbol{\xi}(s)=\mathbf{f}(s);\ \ \mathbf{Z}(s)=\mathbf{I}s^2+\mathbf{B}s+\mathbf{K} \tag{13}$$

Figure 4 shows the structure of visual impedance control considered for the case of fictitious forces. For non-contact tasks, a fictitious force is defined as a function of the distance of the robot's end effector relative to the object of interest on the image plane, as represented in Figure 5, following the authors' proposal.[13]

For obstacle-avoidance tasks, the fictitious force $\mathbf{f}_f$ can be defined in relation to Figure 5 as follows,

$$\mathbf{f}_f=\delta k(\mathbf{d}-\mathbf{r})\begin{cases}\delta=0 & if\ \|\mathbf{d}\|>\|\mathbf{r}\| \\ \delta=1 & if\ \|\mathbf{d}\|<\|\mathbf{r}\|\end{cases} \tag{14}$$

where a repulsion region has been considered within a distance r from the object.

In order to obtain the modified features reference $\boldsymbol{\xi}_o$ (see Figure 4), the compliance vector, $\boldsymbol{\xi}_a=\mathbf{Z}^{-1}\mathbf{f}_f$, is subtracted from the desired features vector,

$$\boldsymbol{\xi}_o(t)=\boldsymbol{\xi}_d(t)-\boldsymbol{\xi}_a(t) \tag{15}$$

Note that, if $\mathbf{f}_f=\mathbf{0}$, which means no interaction with the environment, then $\boldsymbol{\xi}_o=\boldsymbol{\xi}_d$ and the visual servo controller makes the features $\boldsymbol{\xi}$ converge to the reference features $\boldsymbol{\xi}_d$ on the image plane.

Assuming that the visual servo controller can reach exactly the modified reference $\boldsymbol{\xi}_o$, then from (15), $\boldsymbol{\xi}_a=\boldsymbol{\xi}_d-\boldsymbol{\xi}=\tilde{\boldsymbol{\xi}}$ and, therefore, from the definition of the compliance vector ξ_a, $\tilde{\boldsymbol{\xi}}=\mathbf{Z}^{-1}\mathbf{f}_f$. Hence, the proposed controller verifies the objective of visual impedance control as stated by Equation (13).

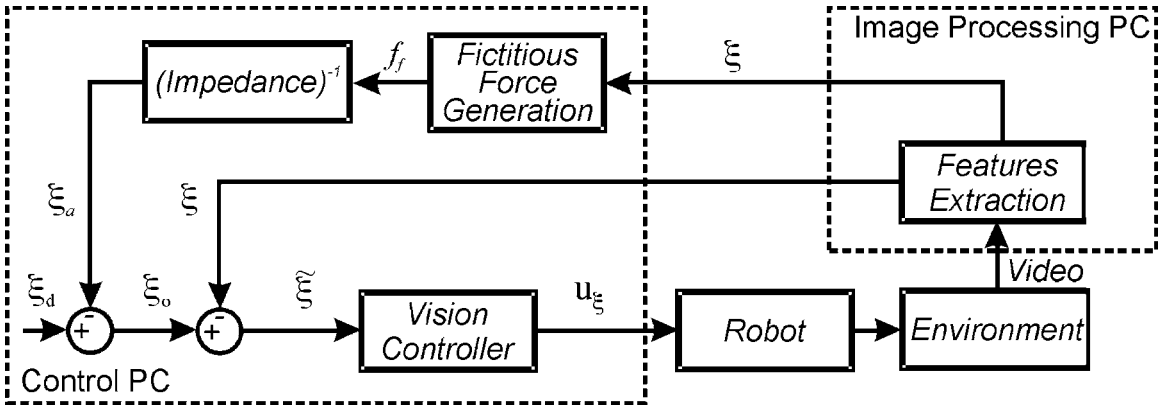


Fig. 4. Vision based impedance control with fictitious forces.

https://doi.org/10.1017/S0263574703005423 Published online by Cambridge University Press

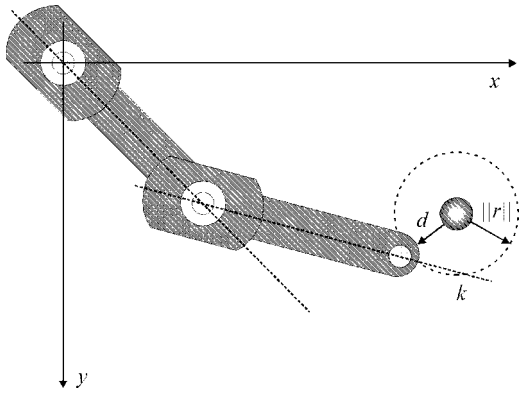


Fig. 5. Generation of fictitious forces.

4. HYBRID SERVO VISUAL CONTROL

The hybrid control scheme originally proposed by Raibert and Craig[20] selects directions in the task space where motion has to be controlled, as well as directions where the interaction force has to be controlled. Control actions on the joints are computed which allow both control objectives to be reached simultaneously. Thus, the control system usually presents two separate control loops for motion and force. Current position is measured on the position control directions, and force is measured on the force control directions. The control corrections are concurrently applied on the joint actuators by the corresponding controllers.

This hybrid control scheme that features controllers based only on position and force measurements can be extended to consider a set of controllers that include, in addition to the traditional force and position controllers, visual servo controllers as well as vision based impedance controllers with fictitious or physical forces as described in the previous sections. Figure 6 shows the general structure, where $C_{1\ldots m}$ represents a set of m controllers (bank of controllers), $\mathbf{S}_{1\ldots m}$ are $n \times n$ diagonal selection matrices and, $Ref_{1\ldots m}$ represent the references set for the sensed variables, which are the necessary ones for each particular controller. Regarding the selection matrices, the diagonal element of $\mathbf{S}_i$ at position j is set to 1 when the controller C_i is active on workspace direction x_j. During each phase of the robot task, only one controller of the bank is selected to control each coordinate direction of the task space. Thus, the summation of all selection matrices $\mathbf{S}_{1\ldots m}$ should give the unit matrix. This hybrid structure extends the well-known position-force hybrid controller to accept other types of controllers, such as the visual based controllers described in the previous sections.

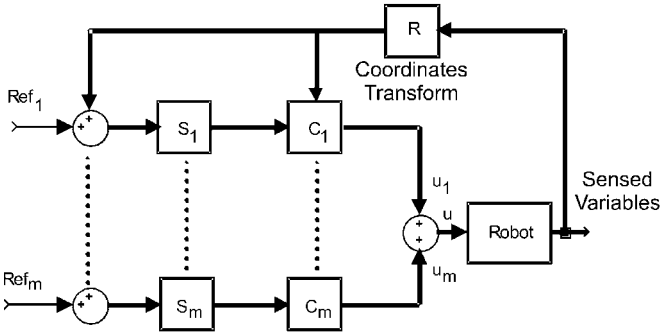


Fig. 6. Bank of controllers.

5. THE INDUSTRIAL ROBOT

5.1 Robot Description

This section describes the industrial robot used for implementing the control algorithms proposed in Sections 2, 3 and 4. To this aim, the BOSCH SR-800 robot with 4 d.o.f. SCARA structure is considered. This manipulator has a control unit supplied by the manufacturer and it is composed of four independent joints and a CPU where a position control algorithm is executed. The position control, as it is usual in industrial robots, includes an internal velocity servo loop.

In order to perform studies by applying various control algorithms on this system, the CPU supplied by the manufacturer has been isolated and replaced for a PC Pentium 133 MHz, where the control algorithms can be programmed. This PC has a data acquisition board linked to the manipulator. In addition, the power stage – servoamplifiers with analog velocity servo – has been kept, which provides a PWM output to the motors and receives, as input, both a reference signal from the control system and the continuous signal supplied by the tachometers of the robot joints. The reference input signal must have a bipolar characteristic, with ± 5 V maximum amplitude. These values correspond to the maximum velocities obtainable for each servomotor in either rotating direction. The control algorithms on the control PC should calculate this reference signal. In addition, there is another computing unit for capturing and processing the images from a camera mounted on the robot's end-effector. Figure 7 depicts the layout of the control scheme.

The control algorithm is performed by user-modifiable software that allows different kinds of controllers to be programmed. The *C*-language programs on MS-DOS platform ensure the real-time execution of algorithms with a 2 ms constant period. Image processing requires 25 ms interval in a MaxPCI workstation from Datacube. This workstation features a 200 MHz Intel Pentium Pro processor with 64Mb RAM, connected to the control PC via an RS232C interface. Images are captured by a CCD Sony video camera, model XC 77-CE.

In addition, the system has an FS6-120 force-torque sensor mounted on the manipulator's wrist. This sensor is linked to the PC via an RS232C interface and through COM1 with a maximum transmission rate of 38400 bauds, whereas COM2 is used for data reception of image features that are transmitted from the workstation devoted to image capturing and processing.

5.2 2-DOF Robot Model

Taking into account that the robot will be commanded by visual feedback on the horizontal-motion plane, the dynamic model for the first two joints of the robot (Figure 8) is considered. Assuming that the voltages applied to the dc drives are the input variables and the joints position and velocities are the state variables of the robot, the following

https://doi.org/10.1017/S0263574703005423 Published online by Cambridge University Press

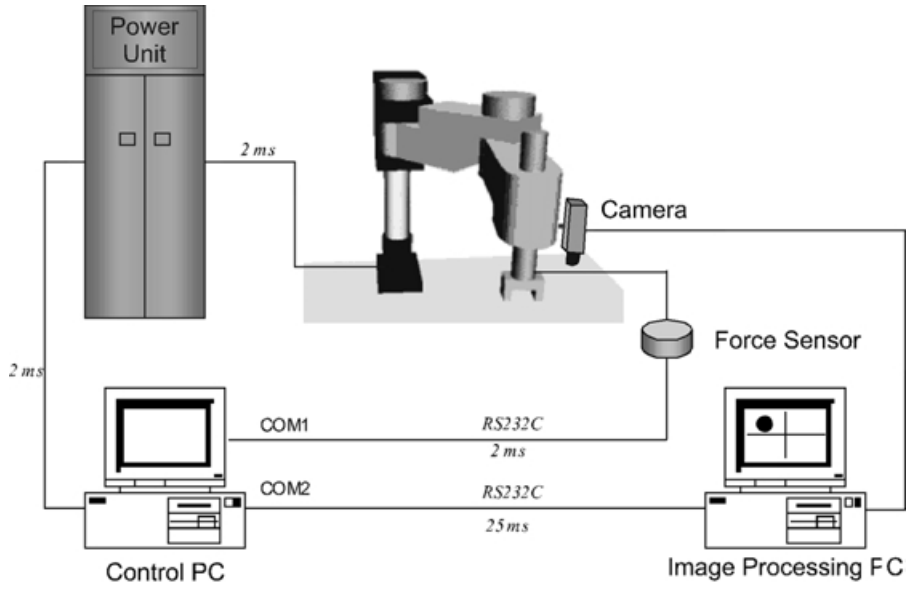


Fig. 7. Layout for the control experiments on the industrial robot.

dynamic model with the structure given in (5) for the 2 dof of the robot can be stated as

$$\begin{bmatrix} J_{m1} & 0 \\ 0 & J_{m2} \end{bmatrix}\begin{bmatrix} \ddot{q}_1 \\ \ddot{q}_2 \end{bmatrix}+\begin{bmatrix} \alpha_1 & 0 \\ 0 & \alpha_2 \end{bmatrix}\begin{bmatrix} \dot{q}_1 \\ \dot{q}_2 \end{bmatrix}+\begin{bmatrix} \beta_1 & 0 \\ 0 & \beta_2 \end{bmatrix}\begin{bmatrix} \tau_1 \\ \tau_2 \end{bmatrix}$$

$$=\begin{bmatrix} \dfrac{1}{\gamma_1 R_1} & 0 \\ 0 & \dfrac{1}{\gamma_2 R_2} \end{bmatrix}\begin{bmatrix} v_1 \\ v_2 \end{bmatrix} \qquad (16)$$

where, for $i=1, 2$

$$\alpha_1 = b_i + \frac{k_{bi}}{\gamma_i}$$

$$\beta_i = \frac{1}{R_i^2}$$

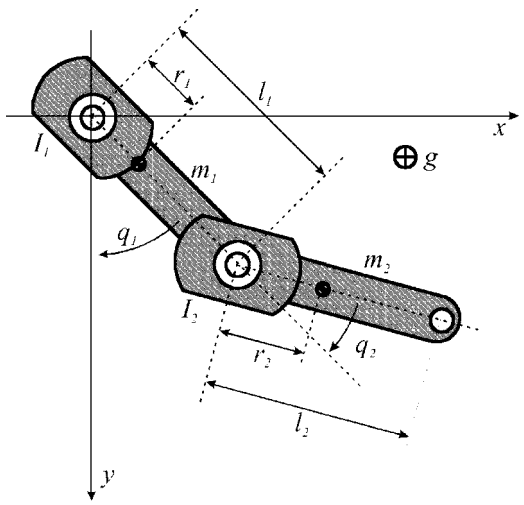


Fig. 8. Two degrees-of-freedom for motion on the horizontal plane.

$$\frac{1}{\gamma_i} = \frac{K_{ai}}{R_{ai}}$$

Parameters of (16) come from the dynamic model of the joint actuators. For a dc motor and by omitting the index $i=1,2$, the well known electrical model is,

$$\tau_m = K_a \cdot i_a$$

$$v = R_a \cdot i_a + L_a \cdot \frac{di_a}{dt} + K_b \cdot \dot{q}_m$$

with τ_m: motor torque; K_a: motor torque constant; i_a: armature current; v: armature voltage; R_a: armature resistance; L_a: armature inductance; K_b: electromotive constant, and q_m: axis position of the motor.

In addition, the mechanical dynamic equation for each actuator is,

$$\mathrm{J_m}\ddot{q}_m = \tau_m - b\,\dot{q}_m - \frac{\tau}{R}$$

$$q_m = R \cdot q$$

where J_m is the motor inertia; b is the viscous friction coefficient of the motor; τ is the coupling torque with the other links on the load side; R is the transmission ratio; and q is the robot's joint position on the load side.

Then, after considering that the mechanical dynamics dominates the electrical one, model (16) can easily be obtained and expressed as a matrix equation like (5). Since the transmission reduction ratios R_1, R_2 are high, the effects of the arm's dynamics can be considered a disturbance on the dominant linear dynamics of the motors.

For the industrial robot considered here, identification experiments using the least-squares method have been carried out for the parameters of model (16), and the results obtained are shown in Table I.[20]

https://doi.org/10.1017/S0263574703005423 Published online by Cambridge University Press

Table I. Values for the identified robot parameters.

J_{m1}	7.499 [Kg.m^2]
J_{m2}	3.544 10^{-4} [Kg.m^2]
γ_1	3.267 [V/Nm]
γ_2	10.101 [V/Nm]
α_1	0.03416 [Nms]
α_2	0.005579 [Nms]
R_1	258.8
R_2	202.5

5.3 Experimental Visual Servo Control Algorithm

According to Section 5.1, the servo-amplifiers of the industrial manipulator should receive speed references generated by the controller. On the other hand, the controller implementation is to be performed on the CPU in the discrete domain. Therefore, from the closed-loop control system equation (6), through a simple difference discrete approximation of the acceleration term, the following approximate discrete equation is inferred,

$$\mathbf{M}(\dot{\mathbf{q}}_k - \dot{\mathbf{q}}_{k-1}) + T_s\mathbf{F}\dot{\mathbf{q}}_k = T_s\mathbf{G}(\mathbf{J}_k^T\mathbf{K}_p\tilde{\boldsymbol{\xi}}_k - \mathbf{K}_v\dot{\mathbf{q}}_k) \qquad (17)$$

where sub-index k indicates the sampling instant and T_s is the sampling period. From Equation (17), the references for the robot's velocity servos described in Section 5.1 are given by,

$$\dot{\mathbf{q}}_k^r = (\mathbf{M} + T_s\mathbf{F} + T_s\mathbf{G}\mathbf{K}_v)^{-1}(T_s\mathbf{G}\mathbf{J}_k^T\mathbf{K}_p\tilde{\boldsymbol{\xi}}_k + \mathbf{M}\dot{\mathbf{q}}_{k-1}^r) \qquad (18)$$

Equation (18), which represents n independent velocity references (one for each joint velocity servo), is the practical control law to be applied to the industrial robot.

6. EXPERIMENTS

The control schemes proposed in Sections 3 and 4 were implemented on the platform developed for the robot BOSCH SR-800 described in Section 5. In order to develop the experiments described below, a 150 mm long peg was mounted on the manipulator's end. The control algorithm programming was written in *C*-language under MS-DOS to allow the control of joints in real time. The sampling frequency was set at 500 Hz, which is the maximum transmission frequency of the force sensor. The error data updating computed on the image is carried out every $T_s = 25\ ms$. Figure 9 shows a view of the experimental set-up.

6.1 Hybrid Force and Vision Based Impedance Control

In this first experiment, the problem of peg insertion with visual guidance is considered. To this aim, the hybrid control structure is used. This includes vision based impedance control with physical force feedback on the horizontal plane and pure-force control on the vertical axis. The visual servo system allows the robot's end to be directed towards the hole for inserting the peg, and the availability of end effector's force feedback on the impedance structure allows small errors of visual guidance to be corrected, which eases the insertion task. Figure 10 shows the diagram of the force-visual impedance hybrid control used in this experience.

On the vertical axis, a proportional-integrative force controller was used, with constants $k_p = 5$, $k_i = 0.01$ and a $10N$

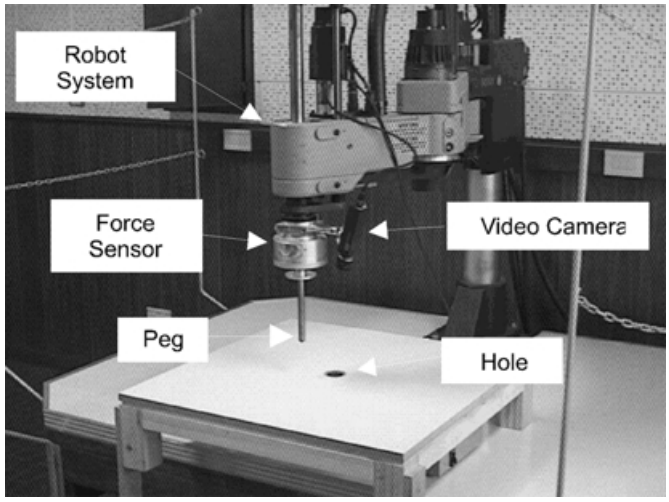


Fig. 9. Experimental set-up.

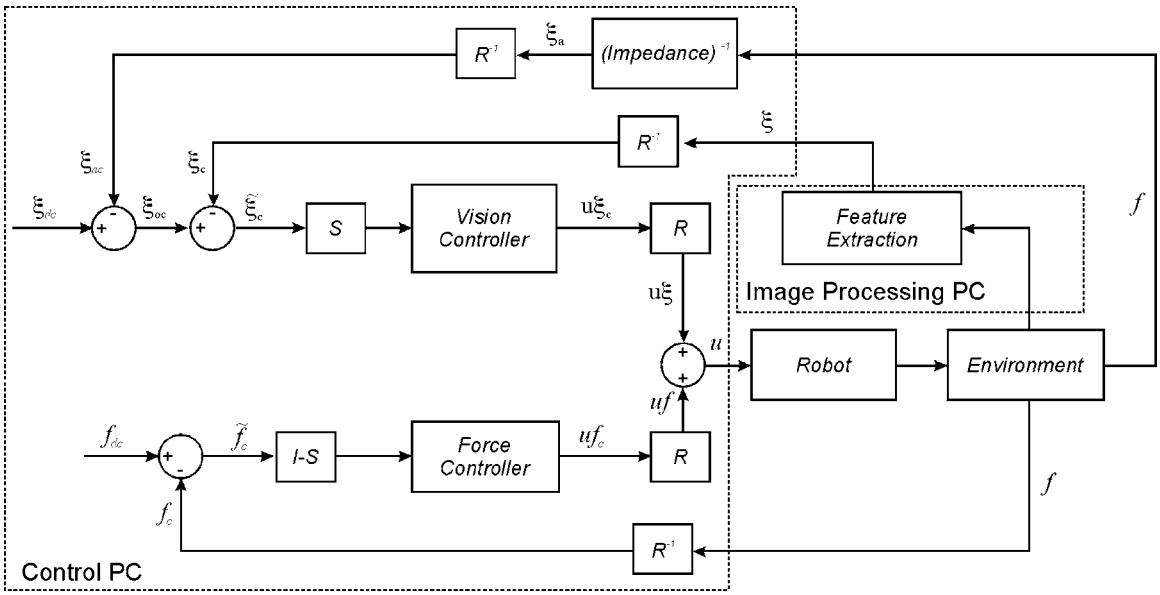


Fig. 10. Control structure for an insertion task.

https://doi.org/10.1017/S0263574703005423 Published online by Cambridge University Press

reference force. For the visual servo controller of Equation (18), the gains used were: $\mathbf{K}_p = diag\{10^{-3}\}$, $\mathbf{K}_v = diag\{6.10^{-4}\}$. In addition, the following values were used for the desired impedance function of Equation (13): $\mathbf{K} = diag\{0.05N/pixel\}$, $\mathbf{B} = diag\{0.01N/pixel.s\}$, $\mathbf{I} = \mathbf{0}$. The values of the desired features on the image plane correspond to the projection of the hole's centre on the image plane when the peg is in position for insertion: $\xi_{xd} = 21$, $\xi_{yd} = -168$ *pixels*. These values can be obtained after a learning experiment, where the operator places the robot in the insertion position and records the image features. Then, the objective of the visual servo control is to make the hole's centre coincide with these reference values on the image plane.

Figure 11 shows the evolution of interaction forces at the robot's end during the insertion task. In the insertion phase, the horizontal forces are fed back to the visual impedance controller so as to fit the peg in the hole and successfully complete the insertion task. The vertical force stabilizes at the 10*N* reference, and the horizontal components accommodate to nonzero values after the insertion. Figure 12 shows the features on the image plane and the norm of the features error in image coordinates. The final positioning error is due to the reference correction imposed by the impedance loop. This experiment shows a successful completion of the insertion task for an unknown position of the hole and a possible misalignment of the peg in the servovisual approaching phase.

6.2 Visual Based Impedance Control with Fictitious Force

In this experiment, the control structure of Figure 4 is considered under a task of the robot's end while avoiding an obstacle on its motion path. The motion is driven by the visual servo control towards a reference located at $\xi_{xd} = 150$, $\xi_{yd} = -150$ *pixels* on the image plane. The 60-*pixel*-diameter cylindrical obstacle is visually detected, generating a fictitious repulsion force that modifies the reference features on the image plane. In order to avoid the obstacle, a 100 *pixels* diameter repulsion zone – or safety zone – was set around the obstacle (Figure 5). The fictitious force was

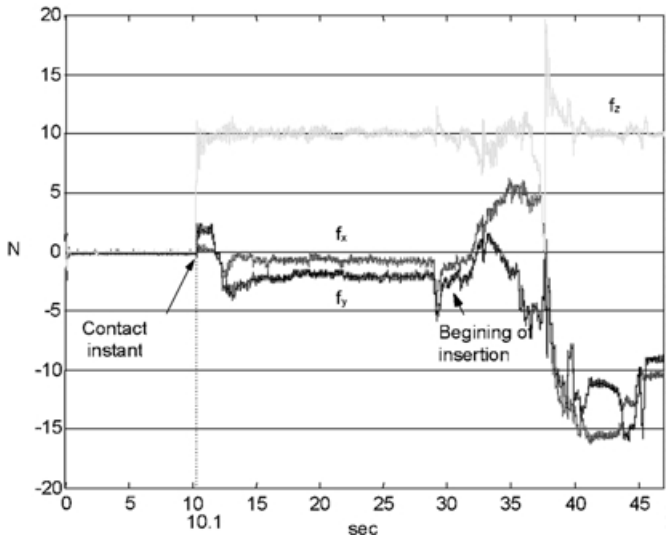


Fig. 11. Evolution of forces. f_x, f_y: horizontal forces, f_z: vertical force.

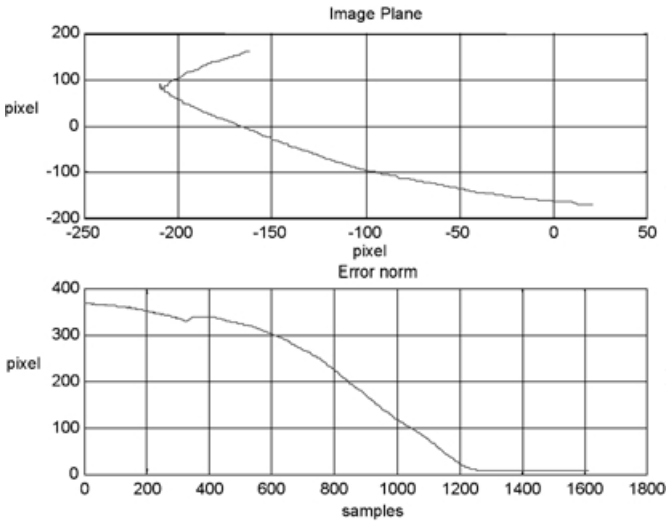


Fig. 12. Evolution of features, and features error norm on the image.

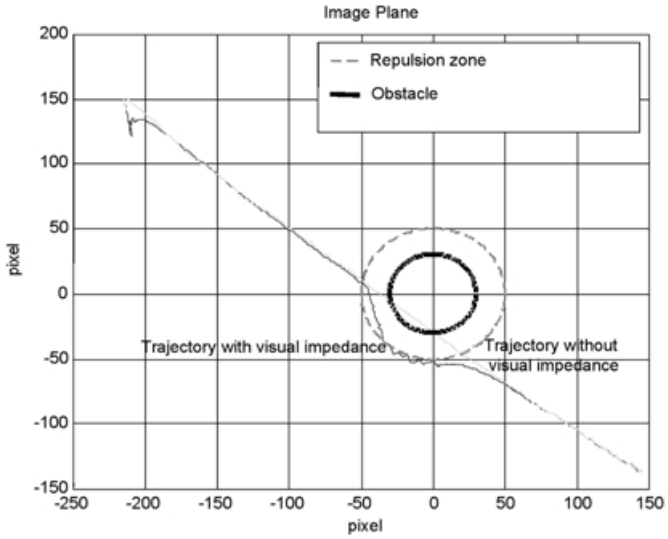


Fig. 13. Evolution of features on the image plane during the task of obstacle avoidance.

generated according to Equation (14) with a constant $k = 0.2N/pixel$. During the experiment, a first-order desired-impedance relationship with constants $\mathbf{K} = diag\{0.2N/pixel\}$ and $\mathbf{B} = diag\{0.07N/pixel.s\}$ was considered. The following gains were selected for the visual servo controller – Equation (18): $\mathbf{K}_p = diag\{15.10^{-4}\}$, $\mathbf{K}_v = diag\{18.10^{-4}\}$.

Figure 13 shows the trajectory of the image features in the process of visually avoiding the obstacle. The solid-line and the dotted-line circles represent the obstacle and the repulsion zone, respectively. The process dynamics of avoiding the obstacle can be regulated by properly choosing the constants for the desired visual impedance. Moreover, the reaction capability to avoid the obstacle is regulated by selecting the constant k in the fictitious repulsion force of equation (14).

7. CONCLUSIONS

This work has presented control structures that allow the combination of force and vision control aiming to perform tasks with a high-level of autonomy. To such an objective,

https://doi.org/10.1017/S0263574703005423 Published online by Cambridge University Press

vision based impedance control structures have been proposed for camera-in-hand robots that carry out the sensorial data fusion of vision and both fictitious and physical forces directly on the image plane. In addition, a hybrid control structure has been considered that allows to select the control on various directions of the task space from a set of controllers that include – besides the traditional motion and force controllers – the visual impedance controllers with fictitious and physical force feedback. The control schemes have been implemented and experimented on a SCARA industrial-type robot in both insertion and obstacle avoidance tasks. These experiments constitute a contribution to the application of these controllers to the industrial robots.

References

1. L. Sciavicco and B. Siciliano. *Modelling and Control of Robot Manipulators* (Springer Verlag, 2000).
2. B. Siciliano and L. Villani, *Robot Force Control* (Kluwer Academic Publishers, 1999).
3. D. Gorinevsky, A. Formolsky and A. Schneider. *Force Control of Robotic Systems* (CRC Press, 1997).
4. J. De Schutter, H. Bruyninckx and M. Spong. "Force control: A bird's eye view", *IEEE International Workshop on Control Problems in Robotics and Automation: Future Directions*, San Diego, CA (1–13, December 1997), 97P075.
5. S. Chiaverini and B. Siciliano. "A survey of robot interaction control schemes with experimental comparison", *IEEE/ASME Trans. on Mechatronics* **4**(3), 273–285 (September 1999).
6. T. Yoshikawa. "Force control of robot manipulators", *Proc. IEEE Int. Conference on Robotics and Automation*, San Francisco, CA (April 2000), pp. 220–226.
7. K. Hashimoto (Editor), *Visual Servoing*. World Scientific Series in Robotics and Automated Systems (World Scientific, 1993), **Vol. 7**.
8. P. Corke, *Visual Control of Robots: High Performance Visual Servoing* (Research Studies Press Ltd, 1996).
9. R. Kelly, R. Carelli, O. Nasisi, B. Kuchen and F. Reyes. "Stable visual servoing of camera-in-hand robotic systems", *IEEE/ASME Trans. On Mechatronics* **5**(1), 39–48, (March 2000).
10. A. Castaño and S. Hutchinson. "Visual compliance: Task-directed visual servo control", *IEEE Trans. on Robotics and Automation* **10**(3), 334–341 (June 1994).
11. T. Tsuji, A. Hiromasa and M. Kaneko. "Non-contact impedance control for redundant manipulators using visual information", *Proc. of the 1997 IEEE Int. Conf. on Robotics and Automation* (Albuquerque, N.M., April 1997), pp. 2571–2576.
12. Y. Nakabo and M. Ishikawa. "Visual Impedance Using 1ms Visual Feedback System", *Proc. of the 1998 IEEE Int. Conference on Robotics & Automation* (Leuven, Belgium, May 1998), pp. 2333–2338.
13. V. Mut, O Nasisi, R. Carelli and B. Kuchen. "Tracking Adaptive Impedance Robot Control with Visual Feedback", *Robotica* **18**, 369–374 (2000).
14. G. Morel, E. Malis and S. Boudet. "Impedance based combination of visual and force control", *Proc. of the 1998 IEEE International Conference on Robotics & Automation* (Leuven, Belgium, May 1998), pp. 1743–1748.
15. B. Nelson and P. Khosla. "Force and vision resolvability for assimilating disparate sensory feedback", *IEEE Trans. on Robotics and Automation* **12**(5), 714–731 (October 1996).
16. K. Hosoda, K. Igarashi and M. Asada, "Adaptive hybrid control for visual and force servoing in an unknown environment", *IEEE Robotics and Automation Magazine* **5**(4), 39–43 (December 1998).
17. M. Takegaki and Y. S. Arimoto. "A new feedback method for dynamic control of manipulators", *ASME J. Dyn. Syst. Meas. Control* **103**, 119–125 (1981).
18. N. Hogan, "Impedance Control: An Approach to Manpulation: Part I, Part II, Part III", *ASME J. Dynamic Syst, Measur. Control* **107**, 1–24 (1985).
19. M. Vidyasagar, *Nonlinear Systems Analysis* (Prentice Hall, 1993).
20. M. Raibert and J. Craig. "Hybrid Position/Force Control of Manipulators", *Journal of Dynamic Systems, Measurement, and Control* **102**, 126–133 (1981).
21. P. A. Muñoz, "Modelling and identification of 2 d.o.f. industrial manipulator", *Technical Report* (In Spanish) (Instituto de Automática, National University of San Juan, Argentina. 2000).

https://doi.org/10.1017/S0263574703005423 Published online by Cambridge University Press